

Large Gravitational Wave Phase Shifts from Strong 3-body Interactions in Dense Stellar Clusters

Kai Hendriks,^{1,2,3,*} Dany Atallah,^{2,3} Miguel Martinez,^{2,3} Michael Zevin,^{4,3} Lorenz Zwick,¹ Alessandro A. Trani,¹ Pankaj Saini,¹ János Takátsy,¹ and Johan Samsing¹

¹*Niels Bohr International Academy, The Niels Bohr Institute,
Blegdamsvej 17, DK-2100, Copenhagen, Denmark*

²*Department of Physics & Astronomy, Northwestern University, Evanston IL 60208, USA*
³*Center for Interdisciplinary Exploration & Research in Astrophysics (CIERA), Evanston, IL*

⁴*Adler Planetarium, 1300 South DuSable Lake Shore Drive, Chicago, IL, 60605, USA*

(Dated: November 14, 2024)

The phase evolution of gravitational waves (GWs) can be modulated by the astrophysical environment surrounding the source, which provides a probe for the origin of individual binary black holes (BBHs) using GWs alone. We here study the evolving phase of the GW waveform derived from a large set of simulations of BBH mergers forming in dense stellar clusters through binary-single interactions. We uncover that a well-defined fraction of the assembled eccentric GW sources will have a notable GW phase shift induced by the remaining third object. The magnitude of the GW phase shift often exceeds conservative analytical estimates due to strong 3-body interactions, which occasionally results in GW sources with clearly shifted and perturbed GW waveforms. This opens up promising opportunities for current and future GW detectors, as observing such a phase shift can identify the formation environment of a BBH, as well as help to characterise the local properties of its surrounding environment.

I. INTRODUCTION

Gravitational wave (GW) templates for binary black hole (BBH) mergers are constructed with the masses, spins, and orbital eccentricities of the progenitor systems. The GW signals from BBHs forming in astrophysical environments rather than isolation are subject to additional modulations, which, if observable, yield a means to probe the environment and formation mechanism of the BBH itself on a single-event basis [e.g. 87]. These modulations include general relativistic propagation effects (e.g., GW source acceleration [e.g. 19, 23, 28, 34, 37, 45, 53, 54, 63, 72, 74, 78, 87, 89–91], GW lensing and gravitational redshift [e.g. 26, 50]), astrophysical environmental effects (e.g., gas dynamical friction [e.g. 11, 93] and tidal forces [63]), and effects beyond classical general relativity (GR) [e.g. 17, 18]. As no BBH merges in a completely empty Universe, such effects should leave imprints in every observed GW signal; however, in most cases the modulations are too small to be resolved. This has led to the key question whether any of the considered BBH merger formation channels such as stellar clusters [7, 9, 10, 38, 48, 51, 52, 55, 57–62, 75, 79, 82, 84], isolated binary stars [13, 14, 20–22, 35, 46, 56, 67–69, 76, 77], active galactic nuclei (AGN) discs [12, 25, 44, 66, 71, 73, 80], or galactic nuclei [6, 8, 27, 29, 30, 39, 40, 47, 70, 81, 83, 85], naturally produce a notable fraction of mergers with measurable GW modulations able to inform about the environment of the merger.

In this *Letter* we perform post-Newtonian (\mathcal{PN}) N-

body simulations (see Methods), to show that BBHs formed through binary-single interactions occurring in dense stellar clusters naturally lead to a well-defined population of GW sources with a measurable GW phase shift caused by the presence of the third object. This is illustrated in Fig. 1, which shows an illustration of different dynamical interactions in a cluster environment (*upper left*), a BH binary-single interaction producing a GW-driven merger (*upper right*), and the corresponding GW phase-shifted signal caused by the presence of the third-object (*lower panel*). Several dynamical pathways can lead to BBH mergers in clusters [e.g. 62], but the pathway relevant for clearly producing phase-shifted sources observable by ground based detectors is characterized by two of the three interacting BHs inspiralling and merge while the third is still bound (Fig. 1 upper right and Fig. 2), also referred to as a *3-body merger* (see Methods). Such 3-body mergers constitute $\sim 10\%$ of the BBH mergers from globular clusters (GCs) [60] and dominate the fraction of eccentric sources, which implies that GW phase-shifted sources will form in notable numbers with observable prospects for both current ground-based GW detectors (LIGO/Virgo/KAGRA) [1–4] and future (Einstein Telescope (ET) [43], Cosmic Explorer (CE) [24]), as well as space-borne detectors (DECIGO/TianQin/Taiji [31, 36, 41, 42] (deci-Hertz) and LISA [5] (milli-Hertz)).

II. GRAVITATIONAL WAVE PHASE SHIFTS

The GW phase shift in 3-body mergers arises from the BBH being bound to the single BH while merging, and therefore moving on a curved orbit with a time-varying velocity along the line-of-sight (LOS) relative to the observer. This creates a time-dependent Doppler shift of

* Corresponding author: kai.hendriks@nbi.ku.dk

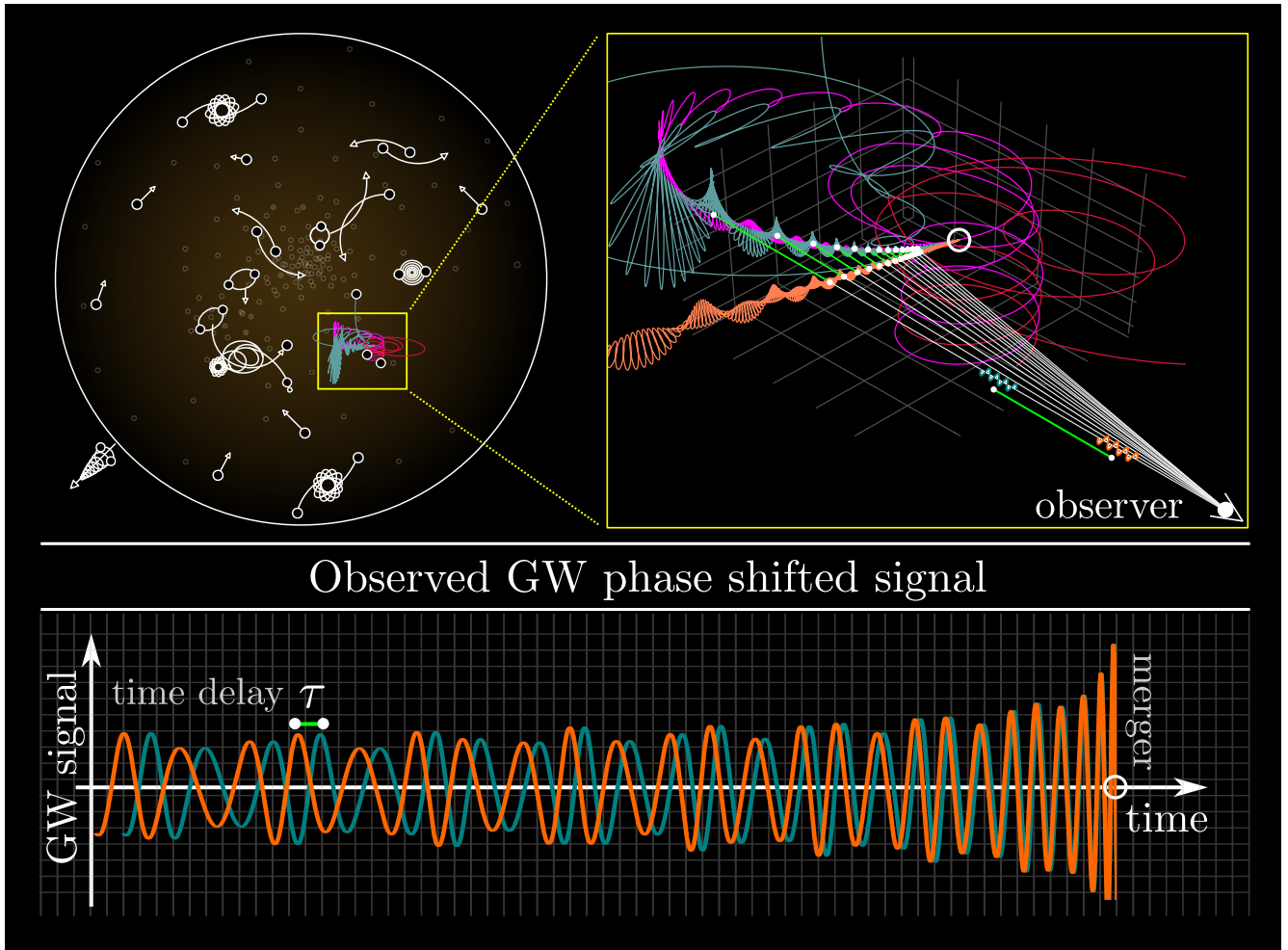


FIG. 1. **Illustration of 3-body interaction resulting in a BBH merger with an observable GW Phase Shift.** *Top left:* A stellar cluster with highlighted BH interactions, each of which is able to produce BBH mergers. *Top right:* Zoom-in on a binary-single interaction resulting in a BBH merger with the third object still bound (3-body merger). *Turquoise-* and *pink* lines show the trajectory of the merging BHs (true path), where the *orange* lines illustrate the path the BBH would have taken without the third object (reference path). The trajectory of the third BH is depicted in *red*. The *white* lines show lines-of-sight for an observer located in the lower right corner, where the *green* lines illustrate the spatial distance between the true- and the reference paths along the sight-lines, respectively. *Bottom:* GW strain as a function of time. The *turquoise* curve shows the GW signal for the observed BBH inspiral (true path), where the *orange* shows what the isolated BBH merger signal would look like (reference path). The two signals are shifted by the light crossing time between the true and the reference BBH paths, i.e. the time it takes the GWs to travel along the green lines. This gives rise to a unique observable GW phase shift that can be directly mapped to the BBH formation and environment.

the GW waveform, which translates to a GW phase shift that can be mapped to the dynamics of the 3-body system [63], analogous to binary pulsar timings [e.g. 45, 63].

In the limit where the acceleration \mathbf{a} of the BBH center-of-mass (COM) near merger from the presence of the third body can be assumed constant, the maximum displacement in time between a GW signal sent from the accelerated BBH path and a non-accelerated path as seen by a distant non-cosmological observer is given by [e.g. 28],

$$\tau(t) = \frac{1}{2} |\mathbf{a}| t^2 = \frac{1}{2} \frac{Gm}{c} \frac{t^2}{R^2}. \quad (1)$$

Here we assume all three BHs have equal mass m , c denotes the speed-of-light, and R refers to the distance between the BBH COM and the single BH at the time of merger (see Methods for solution to the unequal mass case). This τ corresponds to the time it takes a light pulse to travel along one of the green lines shown in Fig. 1; a time that often is referred to as the *Roemer Delay*. From τ , the GW phase shift ϕ , which is the difference in angular cycles of the GW signal in units of radians, can now be expressed as [63]

$$\Delta\phi(t) \approx 2\pi \frac{\tau(t)}{T(t)} \approx \frac{\sqrt{2}}{2} \frac{G^{3/2} m^{3/2}}{c R^2} \times \frac{t^2}{a(t)^{3/2}}, \quad (2)$$

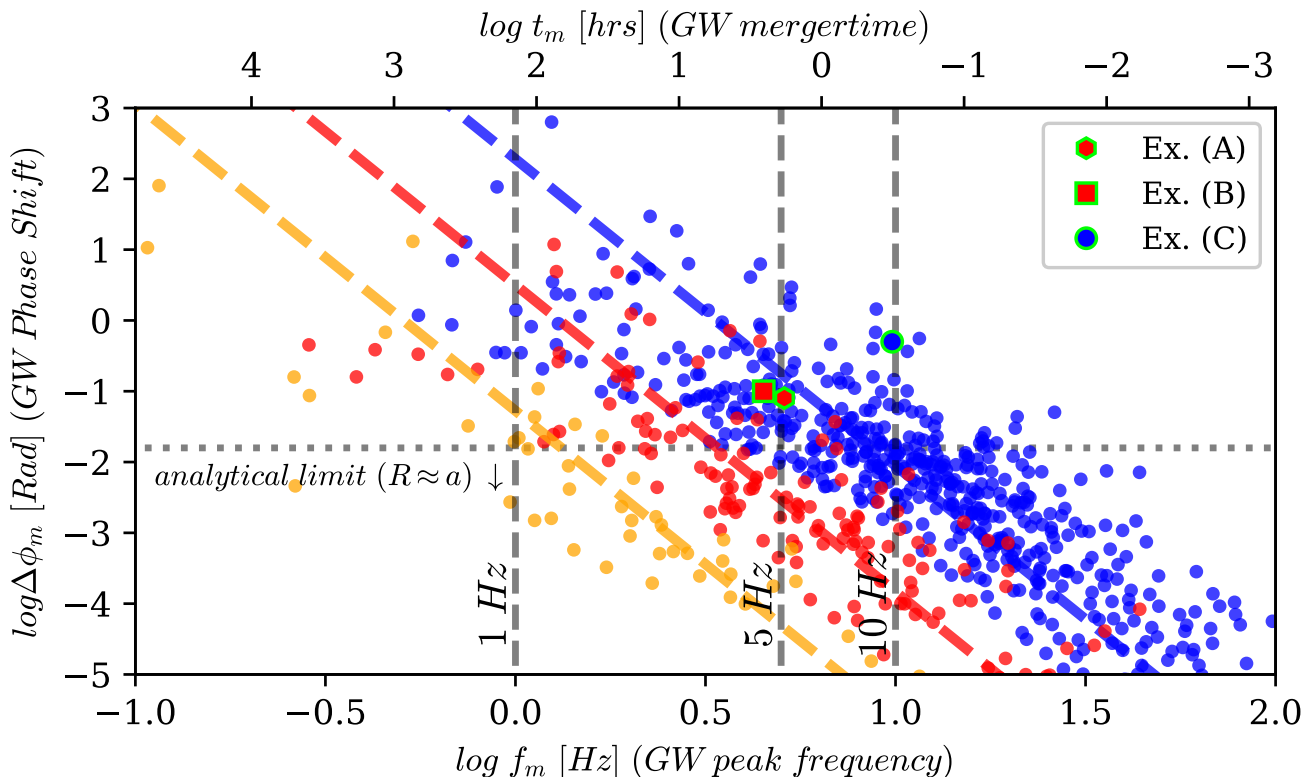


FIG. 2. **Distribution of maximum GW phase shifts from 3-body BBH mergers.** Results from \mathcal{PN} simulations between a BBH and a single incoming BH that concludes with two of the three BHs merging while the third BH is still bound (see Fig. 1 and Fig. 3). Each dot shows the *maximum observable GW phase shift* (y-axis) for each of these mergers, as a function of the corresponding GW peak frequency (bottom x-axis) or merger time (top x-axis), derived using the methods outlined in Sec. II. Each colour refers to a different SMA of the initial BBH before interaction: ~ 1 AU (orange), ~ 0.1 AU (red), and ~ 0.01 AU (blue). The dashed coloured lines illustrate the asymptotic limit $\Delta\phi \propto f^{-13/3}$, where the horizontal dotted line indicates the analytical maximum value for $\Delta\phi$ assuming the distance between the BBH and the single BH, R , is similar to the initial SMA, a (see Methods). The three highlighted examples, (A,B,C), are shown and studied further in Fig. 3.

where $T(t)$ and $a(t)$ denote the BBH orbital time and the BBH semi-major axis (SMA), respectively, at time t . Using the analytical framework of [49], hereafter referred to as *Peters64*, for relating the time t to the BBH's eccentricity, e , and SMA, a , as well as the relation for $a(e)$, one now finds (see Methods),

$$\Delta\phi(e) \approx \frac{144}{85^2 g(1)^{13/2}} \frac{c^9}{G^{9/2}} \times \frac{1}{R^2} \frac{r_0^{13/2}}{m^{9/2}} \times e^{78/19} (1-e^2)^{1/2} g(e)^{13/2}, \quad (3)$$

where $g(e) = (1 + 121e^2/304)^{870/2299}$, and r_0 is the pericenter distance of the merging BBH at the time of formation during the interaction. This r_0 maps to a corresponding GW peak frequency as [e.g. 60]

$$f_0 \approx \frac{1}{\pi} \sqrt{2Gm/r_0^3}, \quad (4)$$

which can be used as a proxy for judging if the BBH is likely to be in the observable band or not (see also

[86]). It should be noted that the definition of the eccentricity in this work is based on the peak harmonic of the orbital frequency [86, 88]. By maximizing the function $e^{78/19} (1-e^2)^{1/2} g(e)^{13/2}$ from Eq. (3), one finds that the GW phase shift $\Delta\phi(e)$ takes its maximum value at eccentricity $e_m \approx 0.95$, with corresponding GW peak frequency (see Methods),

$$f_m \approx f_0 \left(\frac{2e_m^{12/19} g(e_m)}{1+e_m g(1)} \right)^{-3/2}. \quad (5)$$

To summarise, given r_0 and R for each individual scattering, one can now estimate the maximum GW phase shift $\Delta\phi(e_m)$ using Eq. (3) and the corresponding f_m using Eq. (5). We now consider this formalism in the scattering experiments described in the following section.

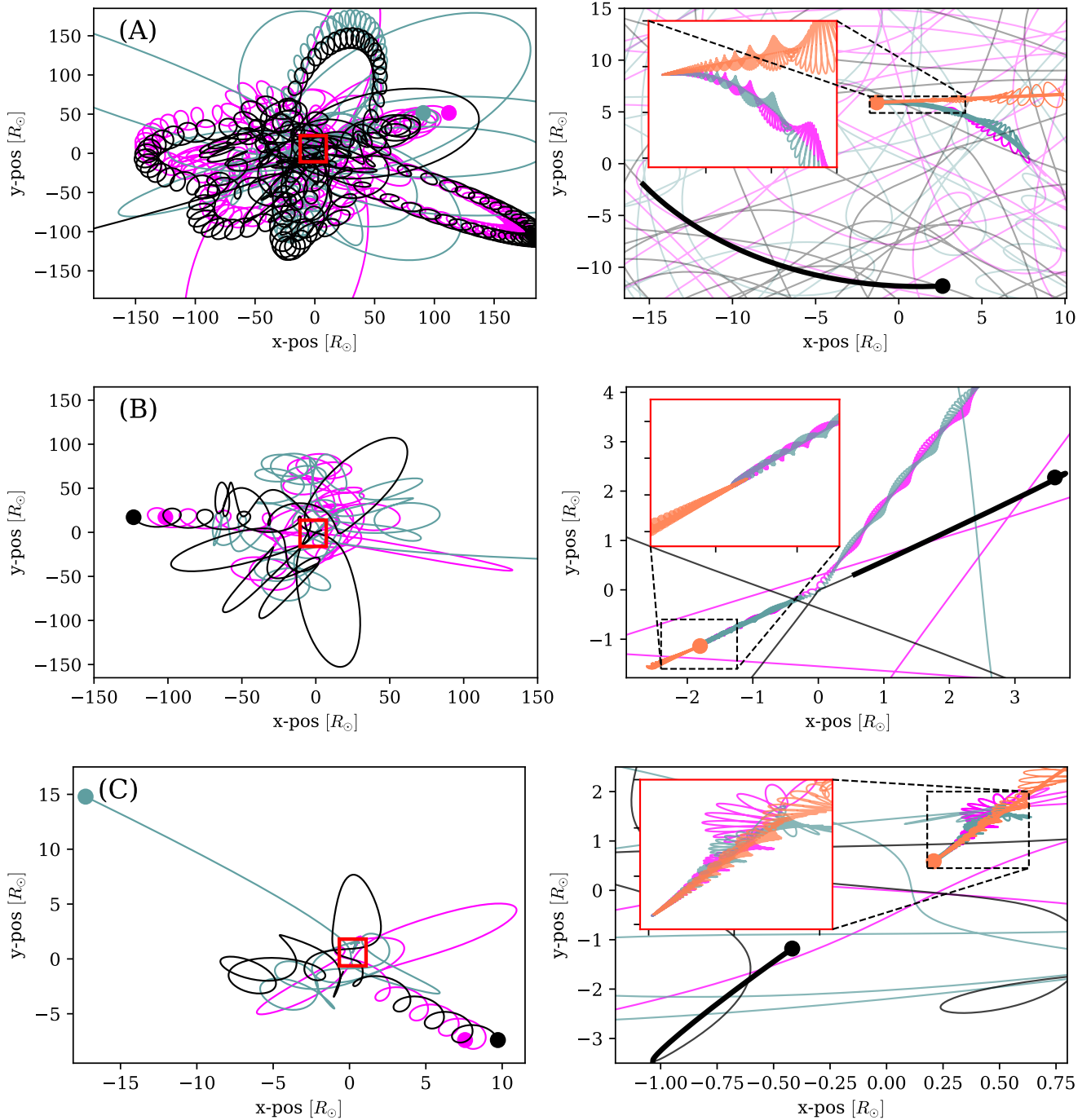


FIG. 3. **Examples of 3-body BBH mergers resulting in significant GW phase shifts.** The shown interactions involve BHs with equal mass $m = 20M_\odot$, and initial SMA $a = 0.1$ AU for case (A) and (B), where case (C) has $a = 0.01$ AU. The filled-circles in the left figures indicate the initial positions of the BHs, where the filled-circles in the right figures show the end positions at merger. The orange lines illustrate the trajectory the merging BBHs would take if the third BH was not there (see Fig. 1). Common for the cases that give rise to significant GW phase shifts is that the chaotic nature of the 3-body problem brings the BBH close to the remaining bound single BH near merger. This is clearly seen in these examples. GW phase shifts and corresponding peak frequencies for (A,B,C) are shown in Fig. 2.

III. RESULTS

We now consider results from controlled \mathcal{PN} binary-single interactions between BBHs with initial SMA $a = 0.01, 0.1, 1$ AU, respectively, and an incoming BH, all with equal mass $m = 20 M_\odot$. These values are characteristic for BHs interacting in dense stellar systems, as these map to stellar clusters with escape velocities, v_e , of $\sim 30 \text{ km s}^{-1}$ (globular cluster), $\sim 90 \text{ km s}^{-1}$ (dense stellar cluster), $\sim 300 \text{ km s}^{-1}$ (nuclear star cluster), for $a = 1, 0.1, 0.01$ AU, respectively [e.g. 6]. For every 3-body merger that forms, we measure numerically r_0 and R , from which we estimate the maximum GW phase shift and corresponding GW peak frequency, as outlined in Section II.

Fig. 2 shows our numerically derived distributions of f_m and $\Delta\phi(e_m)$. As seen, the chaotic nature of the binary-single problem leads to GW sources with notable GW phase shifts, especially in the range between 1 – 10 Hz, accessible to third-generation (3G) ground-based GW observatories such as ET and CE. This is non-trivial, as an analytical estimate for the maximum GW phase shift results in a near universal upper limit of $\Delta\phi_H(e) \sim 10^{-2} \times (m[M_\odot]/R[\text{AU}])^{1/7}$ radians [63], which is derived using Eq. 3 with r_0 set to its maximum possible value, corresponding to where the merging BBH starts exactly at its Hill sphere relative to the single BH at distance R (see Methods).

To understand what kind of 3-body evolutions are able to bypass the analytical limit of $\sim 10^{-2}$ radians, we now consider the three distinct examples shown in Fig. 3. In **(A)**, we show a highly chaotic and longlived interaction, that concludes with an endstate characterized by the BBH passing the bound single near closest approach on a clearly curved orbit. In **(B)**, we show an example where the BBH merges right after turning around to directly move towards the bound single. This creates a large offset between the reference- and the true trajectory. Note also how the single BH scatters off the BBH near the 3-body COM (0, 0) as it inspirals. This creates large extra perturbations to the GW signal. In **(C)**, we show a case where the merging BBH is heading directly towards the bound single BH. Here there is no significant curvature, but the acceleration along its direction of motion towards the single BH creates the GW phase shift.

As follows from Eq. 3, the only important parameter that can freely vary during interactions, and also lead to a large GW phase shift at a given f , is the distance R . The GW sources we see forming with the largest GW phase shift are therefore all characterized by having the remaining single BH much closer at merger than expected from the initial binary separation. As illustrated, this all follows naturally from the chaotic nature of the 3-body problem, which further opens up for new directions in performing, classifying and identifying GW phase-shifted sources in \mathcal{PN} few-body scatterings.

GW phase shifts being a natural outcome when BBHs merge through few-body interactions in stellar clusters

opens up tremendous possibilities for probing the origin and assembly mechanisms of individual GW sources. In particular, future ground-based GW observatories such as ET and CE are not only expected to operate down to a few Hz where many of these sources form, but will also be up to $\mathcal{O}(10\text{--}100)$ times more sensitive than the current LIGO-Virgo-KAGRA (LVK) detector network. This could push down the GW phase shift detection threshold to $\sim 10^{-2}$ radians, and thereby truly open up inference on dynamical mechanisms that bring BBHs to merger throughout the Universe.

ACKNOWLEDGMENTS

The authors are grateful to Lorenzo Speri, Fabio Antonini and Daniel J. D’Orazio for useful discussions. K.H, L.Z., P.S., J.T, and J.S. are supported by the Villum Fonden grant No. 29466, and by the ERC Starting Grant no. 101043143 – BlackHoleMergs led by J. Samsing. M.Z. gratefully acknowledges funding from the Brinson Foundation in support of astrophysics research at the Adler Planetarium. A.A.T. acknowledges support from the Horizon Europe research and innovation programs under the Marie Skłodowska-Curie grant agreement no. 101103134.

IV. METHODS

A. Analytical Framework

Our analytical framework presented in Sec. II builds on the 2.5 \mathcal{PN} orbital averaged equations presented by Peters64. Despite these only including the lowest order \mathcal{PN} terms and using Newtonian definitions of the orbital elements [e.g. 92], these equations still offer very useful insight into the general scalings of the problem, as well as a reliable and fast way of estimating the GW phase shift of 3-body mergers. Once identified, these can then be followed up using more sophisticated analysis methods (see Sec. III and [63]).

For deriving the relations in Sec. II, we make use of the formalism from [28, 63], which presented analytical closed-form solutions to the limit where the acceleration of the eccentric inspiraling BBH is assumed constant, also referred to here as the *linear limit*. We further focus on the maximum possible GW phase shift, denoted by $\Delta\phi$, which is related to the observer dependent value given by $\delta\phi \approx \Delta\phi \times \cos(i)\sin(j)$, where i is the angle in the plane of the ‘outer binary’ (the binary composed of the BBH and the single BH) between the LOS of the observer and the line connecting the location of BBH merger and the COM of the 3-body system, and j is the angle between the LOS and the angular momentum vector of the ‘outer binary’ [e.g. 45, 63].

We start by noting that the time dependent GW phase shift can be approximated by the light crossing time

between the perturbed (accelerated path) and the unperturbed (linear path), defined by τ , divided by the orbital time of the inspiraling BBH, T , times 2π (see Fig. 1). In the limit where the acceleration on the COM of the inspiraling BBH is assumed constant, one therefore finds that $\Delta\phi$ can be written as [63]

$$\Delta\phi(t) \approx 2\pi\tau(t)/T(t). \quad (6)$$

Now using that the time shift (see Fig. 1)

$$\tau(t) = \frac{l(t)}{c} = \frac{1}{2} \frac{Gm_3}{c} \frac{t^2}{R^2}, \quad (7)$$

and the orbital time $T(t)$ is given by

$$T(t) = 2\pi\sqrt{a(t)^3/Gm_{12}}, \quad (8)$$

one finds that $\Delta\phi$ can be written as,

$$\Delta\phi \approx \frac{1}{2} \frac{G^{3/2}}{c} \frac{m_3 m_{12}^{1/2}}{R^2} \times \frac{t^2}{a(t)^{3/2}}, \quad (9)$$

where $a(t)$ is the SMA of the BBH at time t , R is the distance between the BBH and the single at the time of merger, m_1, m_2, m_3 are the masses of the two BBH components and the the single BH, respectively, and $m_{12} = m_1 + m_2$ is the total mass of the BBH. As the GW phase shift is defined as a function of time leading up to merger, the time t can be replaced by the merger time in the rest frame of the BBH. For this we approximate the merger time by the expression given by Peters64,

$$t_e \approx \frac{3}{85} \frac{c^5}{G^3} \frac{a^4(1-e^2)^{7/2}}{m_1 m_2 m_{12}}, \quad (10)$$

where e is the eccentricity of the BBH. By now using the relation between a and e as presented in Peters64,

$$a(e) = \frac{C_0 e^{12/19}}{(1-e^2)} \times g(e), \quad (11)$$

where

$$g(e) = (1 + 121e^2/304)^{870/2299}, \quad (12)$$

and C_0 is a constant that depends on the initial conditions, a_0, e_0 , we can now replace the dependence of a with eccentricity e in the above relations. For determining C_0 we note that the 3-body BBH mergers we consider all start with high eccentricity ($e_0 \approx 1$), from which it follows that the constant $C_0 \approx 2r_0/g(1)$, where $r_0 = a_0(1-e_0)$. With this constant we can now write the relation $a(e)$ as,

$$a(e) \approx \frac{2r_0 e^{12/19}}{(1-e^2)} \frac{g(e)}{g(1)}, \quad (e_0 \approx 1). \quad (13)$$

By substituting this relation between a and e into Eq. 9 and Eq. 10, one finds

$$\begin{aligned} \Delta\phi(e) &\approx \frac{288\sqrt{2}}{85^2 g(1)^{13/2}} \frac{c^9}{G^{9/2}} \times \frac{m_3}{R^2} \frac{r_0^{13/2}}{m_1^2 m_2^2 m_{12}^{3/2}} \\ &\times e^{78/19} (1-e^2)^{1/2} g(e)^{13/2}, \end{aligned} \quad (14)$$

which also can be written in terms of the peak GW frequency at formation,

$$f_0 \approx \frac{1}{\pi} \sqrt{Gm_{12}/r_0^3}. \quad (15)$$

Note here that both e and f , which are key GW observables, are somewhat subject to definitions as recently discussed in [86].

A useful property of r_0 is that it only varies very little during the eccentric inspiral phase, in contrast to a, e . This implies that r_0 can be defined relatively accurately without specifying exactly at what point in time it is defined, as long as the BBH is still eccentric enough, or equivalently close enough to its initial assembly. We elaborate further on this in the Sec. IV C.

Considering Eq. 14, we see that the only part of the function that relates to the time-evolving BBH is the function

$$F(e) = e^{78/19} (1-e^2)^{1/2} g(e)^{13/2}, \quad (16)$$

which has a maximum that defines the maximum of the time-evolving GW phase shift. The eccentricity that leads to this maximum, referred to as e_m , is $e_m \approx 0.95$ (see also [63]) with a corresponding GW peak frequency, $f_m = f(e_m)$, that follows from combining Eq. 13 and 15,

$$f \approx f_0 \times \left(\frac{2e^{12/19} g(e)}{1+e} \frac{g(1)}{g(1)} \right)^{-3/2}. \quad (17)$$

The value for f_m can be below the observable band (see Fig. 2), and to quantify the maximum measurable value for $\Delta\phi$ when the BBH enters the band one therefore needs to rewrite Eq. 9 in terms of f instead of e . However, it is not algebraically possible to express e as a function of f using Peters64's relations. For this, we therefore need to make an approximation in the limit $e \approx 1$ limit for which we can write Eq. 17 as $(f/f_0)^{-2/3} \approx e^{12/19}$ that leads to $e \approx (f_0/f)^{19/18} \approx (f_0/f)$. Substituting this into Eq. 14 one finds,

$$\begin{aligned} \Delta\phi(f) &\approx \frac{c^9 G^{-7/3}}{2\pi^{13/3}} \left(\frac{5}{256} \right)^2 \times \frac{m_3}{R^2} \frac{m_{12}^{2/3}}{m_1^2 m_2^2} \\ &\times f^{-13/3} \times (1 + (f_0/f))^7 (1 - (f_0/f))^{1/2}. \end{aligned} \quad (18)$$

The $\propto f^{-13/3}$ factor correctly defines the asymptomatic limit ($f \gg f_0$), as this is the solution to the well studied circular case [45]. Despite the approximation used between e and f above, we find this expression to correctly capture the GW phase shift evolution within a factor of unity of our considered eccentric inspiraling BBH, as a function of f (see also [63]).

Fig. 4 shows the $\Delta\phi(f)$ evolution of the inspiraling BBHs from our data presented in Fig. 2, with a maximum $\Delta\phi > 10^{-2}$ radians evolved using Eq. 18 from their initial formation frequency f_0 , towards higher f . The dots at the individual peaks are identical to $\Delta\phi(e_m)$, f_m , and derived from Eq. 14 and Eq. 17 (the slight offsets

are due the approximations we here made for $\Delta\phi(f)$. As seen, several of the BBH sources that peak at low f are still able to enter higher frequency bands but with a smaller $\Delta\phi$. Irrespective of 3G GW detectors (ET, CE) will operate down to 1 or 5 Hz, this clearly shows that GW sources will enter, or even form in 3G GW detectors, and possibly also in current LVK-detectors with a significant GW phase shift.

B. Dynamical Constraints

In our considered linear limit it appears from Eq. 14 that any GW phase shift can be achieved, as long as R and r_0 are chosen to be small and large enough, respectively. However, by imposing a dynamical stability to the system, our linear limit also implies a maximum value for $\Delta\phi$ as a function of m and R . To see this we note that r_0 cannot take any value, but has to be small enough that the radiated energy over the first peri-center passage,

$$\Delta E_0 \approx \frac{85\pi G^{7/2} m_1^2 m_2^2 \sqrt{m_{12}}}{12\sqrt{2}c^5 r_0^{7/2}}. \quad (19)$$

leads to an orbital energy

$$E_0 = \frac{Gm_1 m_2}{2a_0}, \quad (20)$$

that has a corresponding SMA a_0 that is smaller than the BBH Hill radius, R_H ,

$$R_H \sim R((m_1 + m_2)/m_3)^{1/3}, \quad (21)$$

by a factor β , such that $a_0 \lesssim \beta R_H$. By now equating E_0 and ΔE_0 , and impose the requirement $a_0 = \beta R_H$ for stability, one finds the following maximum possible value for r_0 , defined here as r_H ,

$$r_H \approx \left(\frac{85\pi}{6\sqrt{2}} \frac{G^{5/2}}{c^5} \frac{\beta R m_1 m_2 m_{12}^{5/6}}{m_3^{1/3}} \right)^{2/7}. \quad (22)$$

The corresponding maximum GW phase shift can now be found by substituting r_H from the above Eq. 22 into Eq. 14,

$$\Delta\phi_H(e) \approx 10^{-2} \times \left(\frac{\beta}{0.1} \right)^{13/7} \left(\frac{m/M_\odot}{R/AU} \right)^{1/7} F(e). \quad (23)$$

As seen here, the maximum value estimated from the characteristic length- and mass-scales of the problem in this linear limit is therefore relatively small, as well as only weakly dependent on the BH mass and initial orbital separation. However, as presented in Sec. III, BBH mergers with GW phase shifts above this limit still exist, and form as a result of the chaotic nature of the 3-body problem, which occasionally brings the BBH much close that $\sim R$ to the single BH near merger (see also Fig. 3).

C. Numerical Methods:

For our scatterings presented in this *Letter*, we use a \mathcal{PN} few-body code that includes the 1-, 2-, and 2.5- \mathcal{PN} terms, where the 1,2- \mathcal{PN} terms are conservative and lead to precession, and the 2.5- \mathcal{PN} term leads to dissipation [15, 16]. Including only the 2.5- \mathcal{PN} term has been shown to be sufficient to statistically resolve the number of mergers forming during the interaction [55], but the 1,2- \mathcal{PN} terms are needed when modeling details of the GW phase shift [63]. The reason is simply that the tidal coupling between the third object and the inspiraling BBH depends on their relative orbital orientations, which will change significantly over the BBH inspiral when the 1,2- \mathcal{PN} terms are included. This tends to dampen the tidal influence from the third object on the BBH in terms of energy and angular momentum transfer, which reduces the possibility for tidally induced GW phase shifts.

For each of our scatterings we initiate a circular BBH with a given SMA a , and sample the distribution of incoming single BHs at infinity according to the system we consider. From the distribution at infinity, we then propagate each single close to the binary using Kepler's equations following well known procedures [33, 65]. At this closer distance we then initiate our \mathcal{PN} few-body code, and let it run for a total of 1000 initial BBH orbital times. This resulted in a few percent of inconclusive scatterings, that mainly originates from scatterings for which the third object is sent out on an almost unbound orbit [e.g. 32, 64]. For each BBH that merges during the interaction, i.e. for each 3-body merger, we measure the peri-center distance r_0 and the distance from the BBH COM to the third object R at merger, from which we theoretically estimate the GW phase shift using the formalism from the above Sec. IV A. The distance r_0 is measured numerically when the inspiraling BBH is subject to a tidal force from the third object that is $< 10^{-3}$ compared to its own binding force. In this way we make sure that tides no longer impact the BBH evolution. The distance r_0 stays approximately constant until the merging BBH starts circularizing, which implies r_0 can be measured relatively unambiguously.

The orange coloured paths seen in Fig. 3 and Fig. 1, which illustrate the trajectories the BBHs would take if the third object was not there, are derived by evolving the \mathcal{PN} equations-of-motion backwards from merger without the third object. This novel technique, as further described in [63] and in Sec. IVD below, allows for an extremely accurate way of numerically estimating observable Doppler- and tidal-effects in the GW signal induced by the presence of the third object. Examples of this is shown in Fig. 5.

D. Numerical Estimation of GW Phase Shifts

The distribution of GW phase shifts shown in Fig. 2 and our analytical descriptions from Sec. II, do not cap-

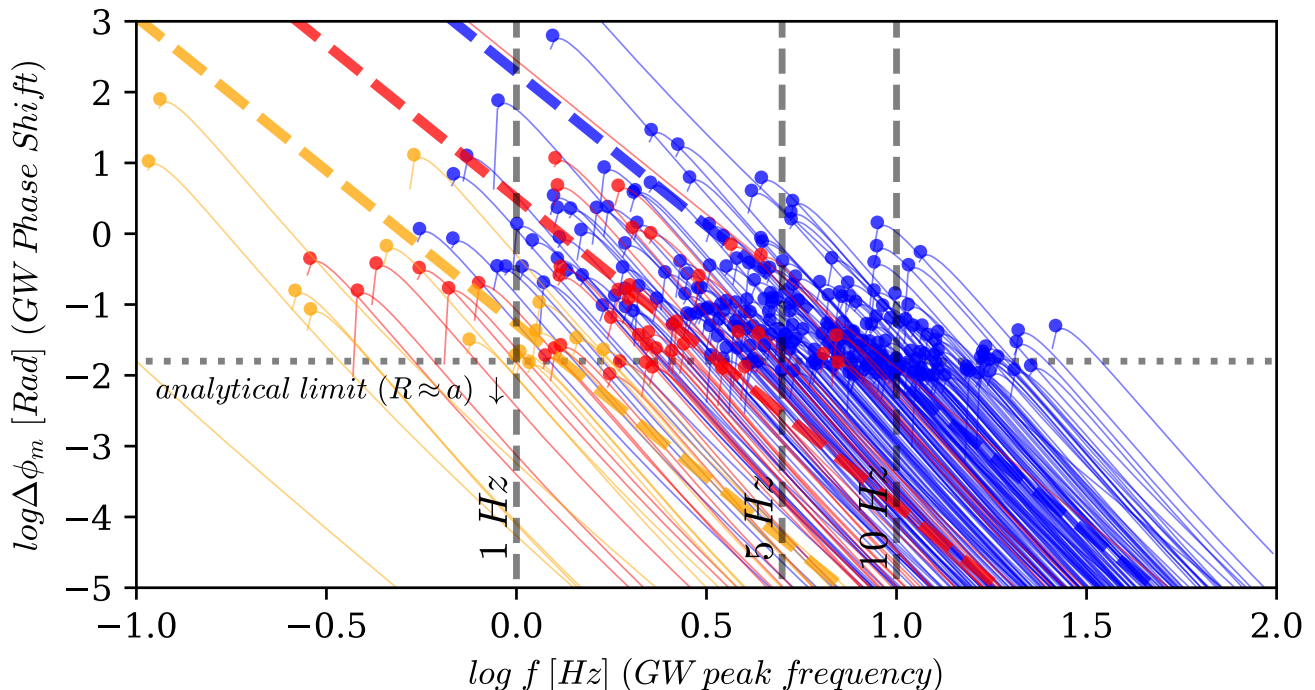


FIG. 4. **Evolution of GW phase shift with GW peak frequency.** The figure shows evolutionary tracks of the GW phase shift as a function of the GW peak frequency, f , from its initial value at formation, f_0 , derived using Eq. 18. The data is the same as the one shown in Fig. 2, but only including the GW sources with a maximum GW phase shift of $> 10^{-2}$. The filled-circles are identical to the ones shown in Fig. 2, and illustrate correctly (within our analytical approximations) the maximum value for the GW phase shift along each track.

ture the rich information that otherwise could be encoded in many of the GW phase shifted sources. For this, one needs numerical methods to resolve the fine and often non-linear differences between the true observed BBH and its corresponding reference GW signal.

As an example, Fig. 3 shows numerically derived quantities for example (A) and (B) presented in Fig. 3. The quantities are derived by comparing the GW signal a distant non-cosmological observer would see from the true BBH evolving near the third object with a reference BBH created by backwards simulating the \mathcal{PN} equations without the third object (Sec. IV C and [63]). In case of example (A), one clearly sees periodic modulations in both the GW peak frequency (*top*), time delay (*middle*), and GW phase shift (*bottom*) below ~ 5000 seconds prior to merger. These originate from the time-dependent tidal

coupling between the single BH and the precessing BBH as its inspirals. When the BBH becomes compact enough the tidal coupling fades away, after which the GW phase shift becomes dominated by the BBH COM acceleration. As seen, this part in the GW phase shift until merger, is very smooth and follows accurately our formalism presented in Sec. II. In example (B) is seen a clear strong perturbation of the GW signal ~ 5000 seconds prior to merger. This is due to the single BH scatters off the BBH close to merger (see Fig. 3), which leads to an almost impulsive change in the BBH orbital parameters. For 3G detectors operating near 5 Hz, such highly non-linear outcomes should be present, and would provide an enormous amount of unique information about the BBH formation beyond the corresponding GW phase shift and linear predictions.

[1] Aasi, J., et al. 2015, *Class. Quant. Grav.*, 32, 074001, doi: 10.1088/0264-9381/32/7/074001
[2] Abbott, B. P., Abbott, R., Abbott, T. D., et al. 2018, *Living Reviews in Relativity*, 21, 3, doi: 10.1007/s41114-018-0012-9
[3] Acernese, F., et al. 2015, *Class. Quant. Grav.*, 32, 024001, doi: 10.1088/0264-9381/32/2/024001

[4] Akutsu, T., et al. 2019, *Nature Astron.*, 3, 35, doi: 10.1038/s41550-018-0658-y
[5] Amaro-Seoane, P., Audley, H., Babak, S., et al. 2017, *ArXiv e-prints*. <https://arxiv.org/abs/1702.00786>
[6] Antonini, F., & Rasio, F. A. 2016, *ApJ*, 831, 187, doi: 10.3847/0004-637X/831/2/187
[7] Askar, A., Szkudlarek, M., Gonddek-Rosińska, D., Giersz,

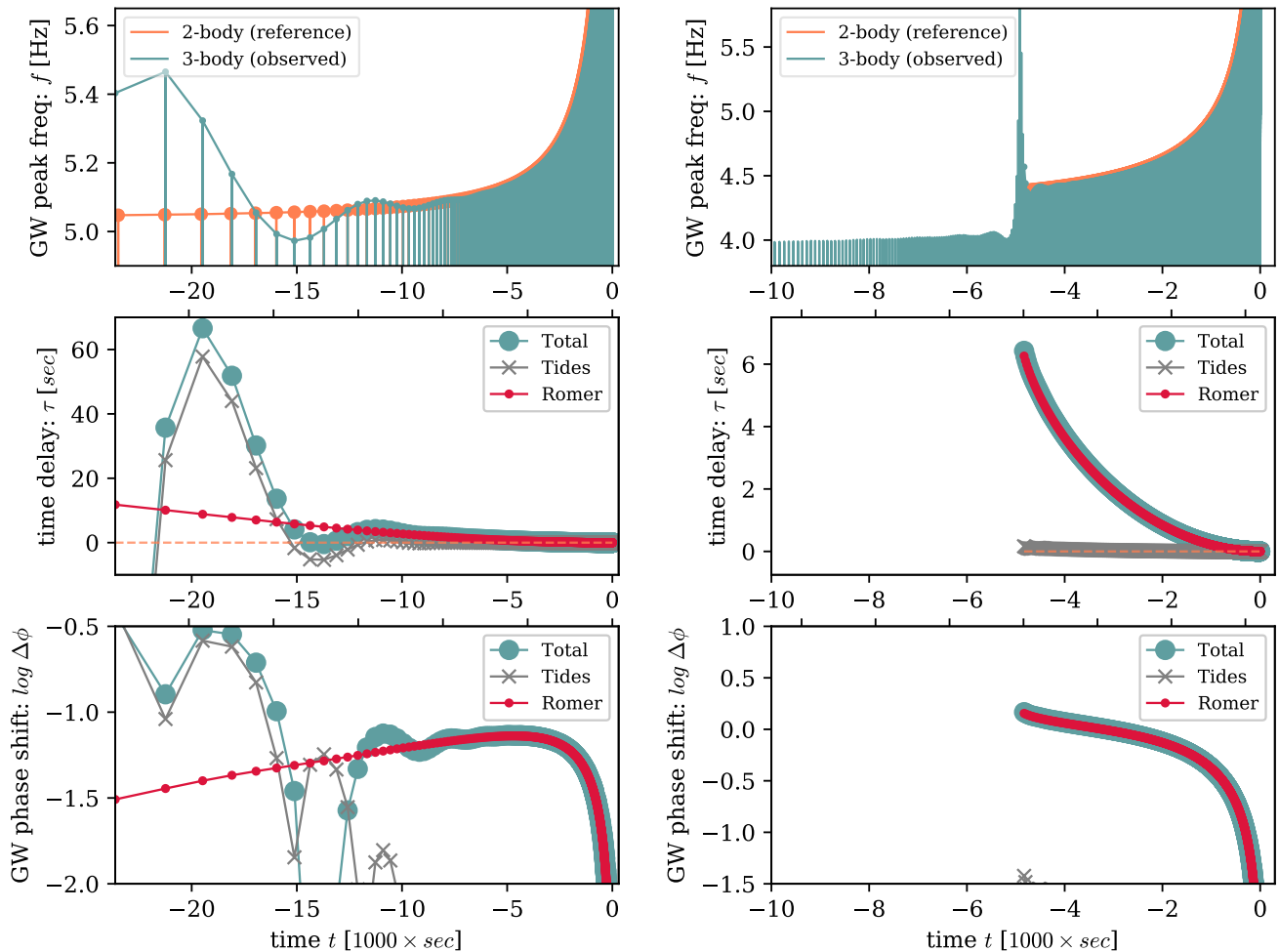


FIG. 5. **GW Modulations in 3-body interactions.** Numerically derived differences, as seen by a distant non-cosmological observer, between the true inspiraling BBH and its reference BBH for the two examples; **(A)** (left column) and **(B)** (right column) introduced in Sec. III. For both columns the *top plot* shows the evolution of BBH peak frequency f (the blue and orange lines show results for the perturbed 3-body BBH and its 2-body reference BBH, respectively), the *middle plot* the time delay τ (the blue line shows the total, the grey line shows the contribution from tides, where the red line is the contribution from the BBH COM acceleration), and in the *bottom plot* is shown the corresponding GW phase shift (same notation as for the middle plot). Our analytical framework from Sec. II describes the evolution shown here with red lines (COM acceleration), where the deviations away from this are caused by semi-chaotic tidal interactions between the single BH and the BBH. Results are further discussed in Sec. IV D.

- M., & Bulik, T. 2017, MNRAS, 464, L36, doi: 10.1093/mnrasl/slw177
- [8] Atallah, D., Trani, A. A., Kremer, K., et al. 2023, MNRAS, 523, 4227, doi: 10.1093/mnras/stad1634
- [9] Bae, Y.-B., Kim, C., & Lee, H. M. 2014, MNRAS, 440, 2714, doi: 10.1093/mnras/stu381
- [10] Banerjee, S., Baumgardt, H., & Kroupa, P. 2010, MNRAS, 402, 371, doi: 10.1111/j.1365-2966.2009.15880.x
- [11] Barausse, E., Cardoso, V., & Pani, P. 2014, Phys. Rev. D, 89, 104059, doi: 10.1103/PhysRevD.89.104059
- [12] Bartos, I., Kocsis, B., Haiman, Z., & Márka, S. 2017, ApJ, 835, 165, doi: 10.3847/1538-4357/835/2/165
- [13] Belczynski, K., Holz, D. E., Bulik, T., & O’Shaughnessy, R. 2016, Nature, 534, 512, doi: 10.1038/nature18322
- [14] Belczynski, K., Repetto, S., Holz, D. E., et al. 2016, ApJ, 819, 108, doi: 10.3847/0004-637X/819/2/108
- [15] Blanchet, L. 2006, Living Reviews in Relativity, 9, 4, doi: 10.12942/lrr-2006-4
- [16] —. 2014, Living Reviews in Relativity, 17, 2, doi: 10.12942/lrr-2014-2
- [17] Camilloni, F., Grignani, G., Harmark, T., et al. 2023, Phys. Rev. D, 107, 084011, doi: 10.1103/PhysRevD.107.084011
- [18] Camilloni, F., Grignani, G., Harmark, T., Orselli, M., & Pica, D. 2023, arXiv e-prints, arXiv:2310.06894, doi: 10.48550/arXiv.2310.06894
- [19] Chamberlain, K., Moore, C. J., Gerosa, D., & Yunes, N. 2019, Phys. Rev. D, 99, 024025, doi: 10.1103/PhysRevD.99.024025

- [20] Dominik, M., Belczynski, K., Fryer, C., et al. 2012, *ApJ*, 759, 52, doi: 10.1088/0004-637X/759/1/52
- [21] —. 2013, *ApJ*, 779, 72, doi: 10.1088/0004-637X/779/1/72
- [22] Dominik, M., Berti, E., O’Shaughnessy, R., et al. 2015, *ApJ*, 806, 263, doi: 10.1088/0004-637X/806/2/263
- [23] D’Orazio, D. J., & Loeb, A. 2020, *Phys. Rev. D*, 101, 083031, doi: 10.1103/PhysRevD.101.083031
- [24] Evans, M., Corsi, A., Afle, C., et al. 2023, arXiv e-prints, arXiv:2306.13745, doi: 10.48550/arXiv.2306.13745
- [25] Fabj, G., & Samsing, J. 2024, arXiv e-prints, arXiv:2402.16948. <https://arxiv.org/pdf/2402.16948>
- [26] Gondán, L., & Kocsis, B. 2022, *MNRAS*, 515, 3299, doi: 10.1093/mnras/stac1985
- [27] Hamers, A. S., Bar-Or, B., Petrovich, C., & Antonini, F. 2018, *ApJ*, 865, 2, doi: 10.3847/1538-4357/aadae2
- [28] Hendriks, K., Zwick, L., & Samsing, J. 2024, arXiv e-prints, arXiv:2408.04603, doi: 10.48550/arXiv.2408.04603
- [29] Hoang, B.-M., Naoz, S., Kocsis, B., Rasio, F. A., & Dosopoulou, F. 2017, ArXiv e-prints. <https://arxiv.org/abs/1706.09896>
- [30] Hong, J., & Lee, H. M. 2015, *MNRAS*, 448, 754, doi: 10.1093/mnras/stv035
- [31] Hu, W.-R., & Wu, Y.-L. 2017, *National Science Review*, 4, 685, doi: 10.1093/nsr/nwx116
- [32] Hut, P. 1983, *AJ*, 88, 1549, doi: 10.1086/113445
- [33] Hut, P., & Bahcall, J. N. 1983, *ApJ*, 268, 319
- [34] Inayoshi, K., Tamanini, N., Caprini, C., & Haiman, Z. 2017, *Phys. Rev. D*, 96, 063014, doi: 10.1103/PhysRevD.96.063014
- [35] Iorio, G., Mapelli, M., Costa, G., et al. 2023, *MNRAS*, 524, 426, doi: 10.1093/mnras/stad1630
- [36] Kawamura, S., Ando, M., Seto, N., et al. 2011, *Classical and Quantum Gravity*, 28, 094011, doi: 10.1088/0264-9381/28/9/094011
- [37] Laeuger, A., Seymour, B., Chen, Y., & Yu, H. 2023, arXiv e-prints, arXiv:2310.16799, doi: 10.48550/arXiv.2310.16799
- [38] Lee, W. H., Ramirez-Ruiz, E., & van de Ven, G. 2010, *ApJ*, 720, 953
- [39] Liu, B., & Lai, D. 2021, *MNRAS*, 502, 2049, doi: 10.1093/mnras/stab178
- [40] Liu, B., Lai, D., & Wang, Y.-H. 2019, *ApJ*, 883, L7, doi: 10.3847/2041-8213/ab40c0
- [41] Liu, S., Hu, Y.-M., Zhang, J.-d., & Mei, J. 2020, *Phys. Rev. D*, 101, 103027, doi: 10.1103/PhysRevD.101.103027
- [42] Luo, J., Chen, L.-S., Duan, H.-Z., et al. 2016, *Classical and Quantum Gravity*, 33, 035010, doi: 10.1088/0264-9381/33/3/035010
- [43] Maggiore, M., Van Den Broeck, C., Bartolo, N., et al. 2020, *J. Cosmology Astropart. Phys.*, 2020, 050, doi: 10.1088/1475-7516/2020/03/050
- [44] McKernan, B., Ford, K. E. S., Bellovary, J., et al. 2017, ArXiv e-prints. <https://arxiv.org/abs/1702.07818>
- [45] Meiron, Y., Kocsis, B., & Loeb, A. 2017, *ApJ*, 834, 200, doi: 10.3847/1538-4357/834/2/200
- [46] Murguia-Berthier, A., MacLeod, M., Ramirez-Ruiz, E., Antoni, A., & Macias, P. 2017, *ApJ*, 845, 173, doi: 10.3847/1538-4357/aa8140
- [47] O’Leary, R. M., Kocsis, B., & Loeb, A. 2009, *MNRAS*, 395, 2127, doi: 10.1111/j.1365-2966.2009.14653.x
- [48] Park, D., Kim, C., Lee, H. M., Bae, Y.-B., & Belczynski, K. 2017, *MNRAS*, 469, 4665, doi: 10.1093/mnras/stx1015
- [49] Peters, P. C. 1964, *Physical Review*, 136, 1224, doi: 10.1103/PhysRev.136.B1224
- [50] Pijnenburg, M., Cusin, G., Pitrou, C., & Uzan, J.-P. 2024, *Phys. Rev. D*, 110, 044054, doi: 10.1103/PhysRevD.110.044054
- [51] Portegies Zwart, S. F., & McMillan, S. L. W. 2000, *ApJ*, 528, L17
- [52] Ramirez-Ruiz, E., Trenti, M., MacLeod, M., et al. 2015, *ApJ*, 802, L22, doi: 10.1088/2041-8205/802/2/L22
- [53] Randall, L., & Xianyu, Z.-Z. 2019, *ApJ*, 878, 75, doi: 10.3847/1538-4357/ab20c6
- [54] Robson, T., Cornish, N. J., Tamanini, N., & Toonen, S. 2018, *Phys. Rev. D*, 98, 064012, doi: 10.1103/PhysRevD.98.064012
- [55] Rodriguez, C. L., Amaro-Seoane, P., Chatterjee, S., et al. 2018, *Phys. Rev. D*, 98, 123005, doi: 10.1103/PhysRevD.98.123005
- [56] Rodriguez, C. L., & Antonini, F. 2018, *ApJ*, 863, 7, doi: 10.3847/1538-4357/aacea4
- [57] Rodriguez, C. L., Chatterjee, S., & Rasio, F. A. 2016, *Phys. Rev. D*, 93, 084029, doi: 10.1103/PhysRevD.93.084029
- [58] Rodriguez, C. L., Haster, C.-J., Chatterjee, S., Kalogera, V., & Rasio, F. A. 2016, *ApJ*, 824, L8, doi: 10.3847/2041-8205/824/1/L8
- [59] Rodriguez, C. L., Morscher, M., Pattabiraman, B., et al. 2015, *Phys. Rev. Lett.*, 115, 051101, doi: 10.1103/PhysRevLett.115.051101
- [60] Samsing, J. 2018, *Phys. Rev. D*, 97, 103014, doi: 10.1103/PhysRevD.97.103014
- [61] Samsing, J., & D’Orazio, D. J. 2018, *MNRAS*, doi: 10.1093/mnras/sty2334
- [62] Samsing, J., D’Orazio, D. J., Kremer, K., Rodriguez, C. L., & Askar, A. 2020, *Phys. Rev. D*, 101, 123010, doi: 10.1103/PhysRevD.101.123010
- [63] Samsing, J., Hendriks, K., Zwick, L., D’Orazio, D. J., & Liu, B. 2024, arXiv e-prints, arXiv:2403.05625, doi: 10.48550/arXiv.2403.05625
- [64] Samsing, J., & Ilan, T. 2018, *MNRAS*, 476, 1548, doi: 10.1093/mnras/sty197
- [65] Samsing, J., MacLeod, M., & Ramirez-Ruiz, E. 2014, *ApJ*, 784, 71, doi: 10.1088/0004-637X/784/1/71
- [66] Samsing, J., Bartos, I., D’Orazio, D. J., et al. 2022, *Nature*, 603, 237, doi: 10.1038/s41586-021-04333-1
- [67] Schröder, S. L., Batta, A., & Ramirez-Ruiz, E. 2018, *ApJ*, 862, L3, doi: 10.3847/2041-8213/aacf8d
- [68] Silsbee, K., & Tremaine, S. 2017, *ApJ*, 836, 39, doi: 10.3847/1538-4357/aa5729
- [69] Spera, M., Mapelli, M., Giacobbo, N., et al. 2019, *MNRAS*, 485, 889, doi: 10.1093/mnras/stz359
- [70] Stephan, A. P., Naoz, S., Ghez, A. M., et al. 2016, *MNRAS*, 460, 3494, doi: 10.1093/mnras/stw1220
- [71] Stone, N. C., Metzger, B. D., & Haiman, Z. 2017, *MNRAS*, 464, 946, doi: 10.1093/mnras/stw2260
- [72] Stokrov, V., Fragione, G., Wong, K. W. K., Helfer, T., & Berti, E. 2022, *Phys. Rev. D*, 105, 124048, doi: 10.1103/PhysRevD.105.124048
- [73] Tagawa, H., Haiman, Z., & Kocsis, B. 2020, *ApJ*, 898, 25, doi: 10.3847/1538-4357/ab9b8c
- [74] Tamanini, N., Klein, A., Bonvin, C., Barausse, E., & Caprini, C. 2020, *Phys. Rev. D*, 101, 063002, doi: 10.1103/PhysRevD.101.063002

- [75] Tanikawa, A. 2013, *MNRAS*, 435, 1358, doi: 10.1093/mnras/stt1380
- [76] Tanikawa, A., Susa, H., Yoshida, T., Trani, A. A., & Kinugawa, T. 2021, *ApJ*, 910, 30, doi: 10.3847/1538-4357/abe40d
- [77] Tanikawa, A., Yoshida, T., Kinugawa, T., et al. 2022, *ApJ*, 926, 83, doi: 10.3847/1538-4357/ac4247
- [78] Toubiana, A., Sberna, L., Caputo, A., et al. 2021, *Phys. Rev. Lett.*, 126, 101105, doi: 10.1103/PhysRevLett.126.101105
- [79] Trani, A. A., Leigh, N. W. C., Boekholt, T. C. N., & Portegies Zwart, S. 2024, *A&A*, 689, A24, doi: 10.1051/0004-6361/202449862
- [80] Trani, A. A., Quaini, S., & Colpi, M. 2023, arXiv e-prints, arXiv:2312.13281, doi: 10.48550/arXiv.2312.13281
- [81] —. 2024, *A&A*, 683, A135, doi: 10.1051/0004-6361/202347920
- [82] Trani, A. A., Rastello, S., Di Carlo, U. N., et al. 2022, *MNRAS*, 511, 1362, doi: 10.1093/mnras/stac122
- [83] Trani, A. A., Spera, M., Leigh, N. W. C., & Fujii, M. S. 2019, *ApJ*, 885, 135, doi: 10.3847/1538-4357/ab480a
- [84] Trani, A. A., Tanikawa, A., Fujii, M. S., Leigh, N. W. C., & Kumamoto, J. 2021, *MNRAS*, 504, 910, doi: 10.1093/mnras/stab967
- [85] VanLandingham, J. H., Miller, M. C., Hamilton, D. P., & Richardson, D. C. 2016, *ApJ*, 828, 77, doi: 10.3847/0004-637X/828/2/77
- [86] Vijaykumar, A., Hanselman, A. G., & Zevin, M. 2024, *ApJ*, 969, 132, doi: 10.3847/1538-4357/ad4455
- [87] Vijaykumar, A., Tiwari, A., Kapadia, S. J., Arun, K. G., & Ajith, P. 2023, *ApJ*, 954, 105, doi: 10.3847/1538-4357/acd77d
- [88] Wen, L. 2003, *ApJ*, 598, 419, doi: 10.1086/378794
- [89] Wong, K. W. K., Baibhav, V., & Berti, E. 2019, *MNRAS*, 488, 5665, doi: 10.1093/mnras/stz2077
- [90] Xuan, Z., Naoz, S., & Chen, X. 2023, *Phys. Rev. D*, 107, 043009, doi: 10.1103/PhysRevD.107.043009
- [91] Yunes, N., Miller, M. C., & Thornburg, J. 2011, *Phys. Rev. D*, 83, 044030, doi: 10.1103/PhysRevD.83.044030
- [92] Zwick, L., Capelo, P. R., Bortolas, E., Mayer, L., & Amaro-Seoane, P. 2020, *MNRAS*, 495, 2321, doi: 10.1093/mnras/staa1314
- [93] Zwick, L., Capelo, P. R., & Mayer, L. 2023, *MNRAS*, 521, 4645, doi: 10.1093/mnras/stad707